Nicotiana benthamiana Methanol-Inducible Gene (MIG) 21 Encodes a Nucleolus-Localized Protein that Stimulates Viral Intercellular Transport and Downregulates Nuclear Import

Ekaterina V. Sheshukova , Kamila Kamarova , Natalia Ershova , Tatiana Komarova *

Posted Date: 13 December 2023

doi: 10.20944/preprints202312.1011.v1

Keywords: methanol; methanol-inducible gene; intercellular transport; inducible promoter; plant resistance

Article

Nicotiana benthamiana Methanol-Inducible Gene (MIG) 21 Encodes a Nucleolus-Localized Protein that Stimulates Viral Intercellular Transport and Downregulates Nuclear Import

Ekaterina V. Sheshukova [1], Kamila A. Kamarova [1], Natalia M. Ershova [1] and Tatiana V. Komarova [1,2,*]

[1] Vavilov Institute of General Genetics Russian Academy of Sciences, 119991, Moscow, Russia
[2] Belozersky Institute of Physico-Chemical Biology Lomonosov Moscow State University, 119991 Moscow, Russia
* Correspondence: t.komarova@belozersky.msu.ru

Abstract: Mechanical damage of plant tissues leads to the activation of methanol production and its release in the atmosphere. The gaseous methanol or vapors emitted by the damaged plant induce resistance in neighboring intact plants to bacterial pathogens but create favorable conditions for the viral infection spread. Among *Nicotiana benthamiana* methanol-inducible genes (MIGs) most are associated with plant defense and intercellular transport. Here we characterize *NbMIG21* that encodes a 209-aa protein (NbMIG21p) which does not share any homology with annotated proteins. NbMIG21p was demonstrated to contain nucleolus localization signals (NoLS). Co-localization studies with fibrillarin and coilin, nucleolus and Cajal bodies marker proteins, revealed that NbMIG21p is distributed between these subnuclear structures. Our results show that recombinant NbMIG21 possess DNA-binding properties. Similar to gaseous methanol effect an increased *NbMIG21* expression leads to the downregulation of the nuclear import of NLS-containing proteins as was demonstrated on the model GFP-NLS protein. Moreover, upregulated *NbMIG21* facilitates tobacco mosaic virus (TMV) intercellular transport. We identified *NbMIG21* promoter (PrMIG21) and showed that it is methanol-sensitive thus induction of *NbMIG21* expression occurs at the level of transcription. Our findings suggest that methanol-activated *NbMIG21* might participate in creating favorable conditions for the viral reproduction and spread.

Keywords: methanol; methanol-inducible gene; intercellular transport; inducible promoter; plant resistance

1. Introduction

Due to attached lifestyle, plants are constantly exposed to abiotic (drought, salinity, heat, cold, lack of nutrients, lack of light, high light intensity) and biotic (viruses, microorganisms, insects, herbivorous animals) environmental stressors [1]. During evolution plants developed two main ways to coordinate generalized defense reactions: intercellular communication via plasmodesmata (PD) and signal transfer by emission and perception of volatile organic compounds (VOCs). PD serve for transport of various regulatory molecules including RNA and proteins in addition to low molecular weight compounds [2]. PD permeability is under strict control and is regulated via several main mechanisms: (i) physical narrowing of the channel by callose depositions mediated by callose-degrading and callose synthesizing enzymes, (ii) regulation by various proteins associated and localized in PD, (iii) signals from mitochondria and chloroplasts that are transferred to the nucleus and affect expression of various genes encoding proteins the ensemble of which defines PD state [3–5]. Therefore, PD regulation usually involves nucleus and nucleus-encoded genes. Pathogenic bacteria and viruses could interfere with plant immune response affecting nucleus and nucleocytoplasmic transport as well as PD and symplastic transport.

To realize intra- and interplant communication in the absence of physical contact, plants utilize VOCs [6,7]. In addition to simple molecules such as oxygen, carbon dioxide and water vapor, plants

 doi:10.20944/preprints202312.1011.v1

emit a huge amount of various complex compounds as terpenoids, derivatives of fatty acids and amino acids, benzoids, phenylpropanoids, etc. into the atmosphere [8]. Gaseous methanol is a product of cell wall pectin demethylation by pectin methylesterase (PME) [9,10]. Methanol is one of the signal molecules that is emitted both in normal conditions [11,12] and in response to stress [13–15]. It plays significant role in plant-herbivores [16,17] and plant-pathogen interactions [18]. Methanol emitted by an injured plant triggers defense responses in both its own intact leaves and neighboring plants: it induces resistance to bacterial pathogens *Agrobacterium tumefaciens* and *Ralstonia solanacearum* [18]. Moreover, it was shown that transgenic plants with *PME* overexpression are characterized by increased level of methanol emission [18] and resistance to polyphagous insect pests [19]. Another research group analyzed transcriptome of transgenic tobacco plants with increased methanol emission [17] and revealed changes in the expression of transcription factors related to plant-herbivore interactions together with cell-wall modifying enzymes. The molecular mechanisms underlying methanol-induced defense response is still mainly unknown. Methanol was demonstrated to activate specific factors, encoded by methanol-inducible genes (MIGs) which participate in the plant's resistance to both biotic stress factors [18,20]. Most of these genes are involved in defense reactions and intercellular transport. Plants treatment with physiological concentration of gaseous methanol leads to activation of intercellular transport of macromolecules and impeded nucleocytoplasmic transport that results in creation of favorable conditions for viral infection as an unintended consequence of the induced antibacterial resistance [18]. Among selected MIGs are *NbAELP* (a gene encoding aldose-1-epimerase-like protein, previously designated as NCAPP) and 1,3-beta-glucanase (BG) that were shown to participate in activation of intercellular transport of macromolecules and stimulation of tobacco mosaic virus (TMV) RNA accumulation [18]. Moreover, NbAELP was demonstrated to affect nucleocytoplasmic transport [21] as well as PME [22].

Plasmodesmata (PD) act as pathways for transporting different compounds such as proteins, nucleic acids, hormones, and metabolites, crucial for signaling during plant development and defense [5]. The flow through PD is controlled by various mechanisms, among which the most extensively studied is callose-dependent regulation of PD permeability via modulation of callose depositions in the cell wall near these channels. Callose turnover is maintained by several enzymes that are involved in callose synthesis, degradation, and stabilization [23]. Furthermore, research into proteins associated with PD [24], the interactions between the endoplasmic reticulum and the plasma membrane (PM) around these channels [25], and the specific lipid composition of the PM within them [26] has broadened our understanding of PD function [27]. Recent evidence suggests that signals from different cell organelles, primarily mitochondria and chloroplasts, also play a role in controlling plasmodesmata. These signals are transmitted to the cell nucleus and impact the expression of genes involved in regulating intercellular transport and plasmodesmata function [4,28,29]. However, the exact mechanisms and components involved in this signaling pathway are still to be elucidated. Therefore, regulation of plasmodesmata involves proteins within the channels themselves as well as signal pathways from organelles to the nucleus.

Previously, among MIGs we have identified gene with an unknown function, designated *NbMIG21* and demonstrated its involvement in regulation of intercellular transport of macromolecules as well as ability to stimulate TMV-based vector reproduction [18]. In the current study we further investigated *NbMIG21* features and functions. We demonstrated that NbMIG21p has nuclear localization and is concentrated in subnuclear structures, in particular, nucleolus. Similar to NbAELP and PME, NbMIG21p interferes with nucleocytoplasmic transport as was demonstrated using GFP-NLS reporter molecule. Moreover, increased *NbMIG21* expression stimulates intercellular transport of TMV-based viral vector. Finally, we have isolated *NbMIG21* promoter region, demonstrated its sensitivity to methanol and shown, that recombinant NbMIG21p has DNA-binding properties being able to bind various promoters including its own one.

Thus we suggested that NbMIG21 could be one of the players participating in organelle-to-nucleus plasmodesmata signaling and affecting both nucleocytoplasmic and intercellular transport. We hypothesize that NbMIG21 might participate in creating favorable conditions for the viral reproduction (i) interfering with nucleocytoplasmic transport of the macromolecules that could

Preprints (www.preprints.org) | NOT PEER-REVIEWED | Posted: 13 December 2023 doi:10.20944/preprints202312.1011.v1

include antiviral cellular factors, (ii) increasing plasmodesmata permeability leading to enhanced viral spread.

2. Results

2.1. Analysis of N. benthamiana Methanol-Inducible Gene 21 (NbMIG21)

Nicotiana benthamiana methanol-inducible gene 21 coding sequence (*NbMIG21,* GenBank Ac GU128961) was identified among genes expression of which increased in response to gaseous methanol or vapors from the wounded plant [18]. Initially *NbMIG21* was isolated from leaves. Here we analyzed *NbMIG21* expression in different parts of the plant as well as in seedlings using quantitative real-time PCR (qRT-PCR) (Figure 1). It appeared that leaves are characterized with the highest level of expression that is in line with results based on transcriptome data from *N. benthamiana* Gene Expression Atlas (http://sefapps02.qut.edu.au/atlas/tREX6.php) resource (Figure S1). Moreover, *NbMIG21* mRNA accumulation in leaves increases with their age.

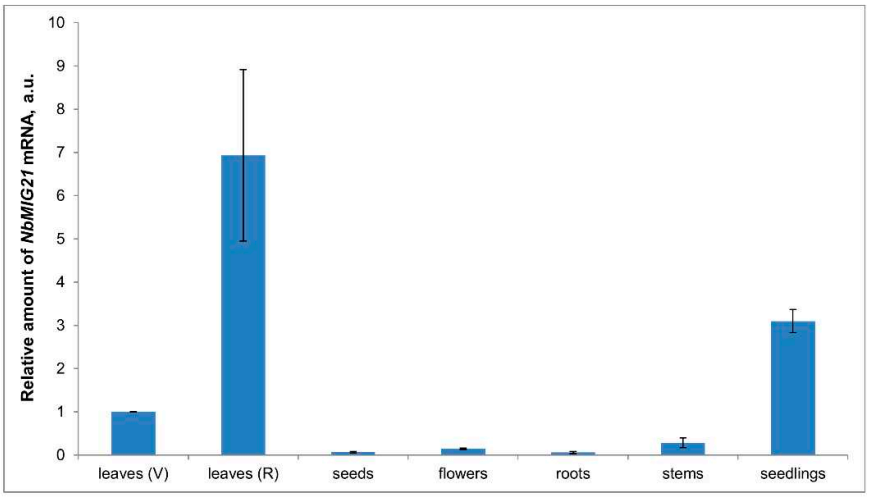

Figure 1. Quantitative RT-PCR analysis of *NbMIG21* expression in different *N. benthamiana* organs and seedlings. Seedlings were grown for 10 d after germination. Leaves (V) were harvested from 3-week-old plants (vegetative stage); leaves (R), stems and flowers were harvested from same plants 5 weeks later (reproductive stage). Seeds were collected from 10-week-old plants. The levels of expression are normalized to the *PP2A* gene. The *NbMIG21* expression level in leaves (V) was taken as 1. The plot represents means ± SE of three technical repeats from three biological replicates each.

 doi:10.20944/preprints202312.1011.v1

A

MASLQCHKPAQHAPSTLCQKTTTVTCNKANNEHHSFADKMKDMTDKMYHHDSHNHQSACHGTKTQQTAACHGTKTQQSA
ACHGTKTQQSAASHRTKTQQTACHGTSANGTKTQLSVACHGTKTQQSAASHGTKTQQTACHGTSATATHARACGKKKEG
SFMHKMRDQMRSRRNRNKDGSCSDGSDSSSSSSSDESDNENCGRTKNRGSC

B

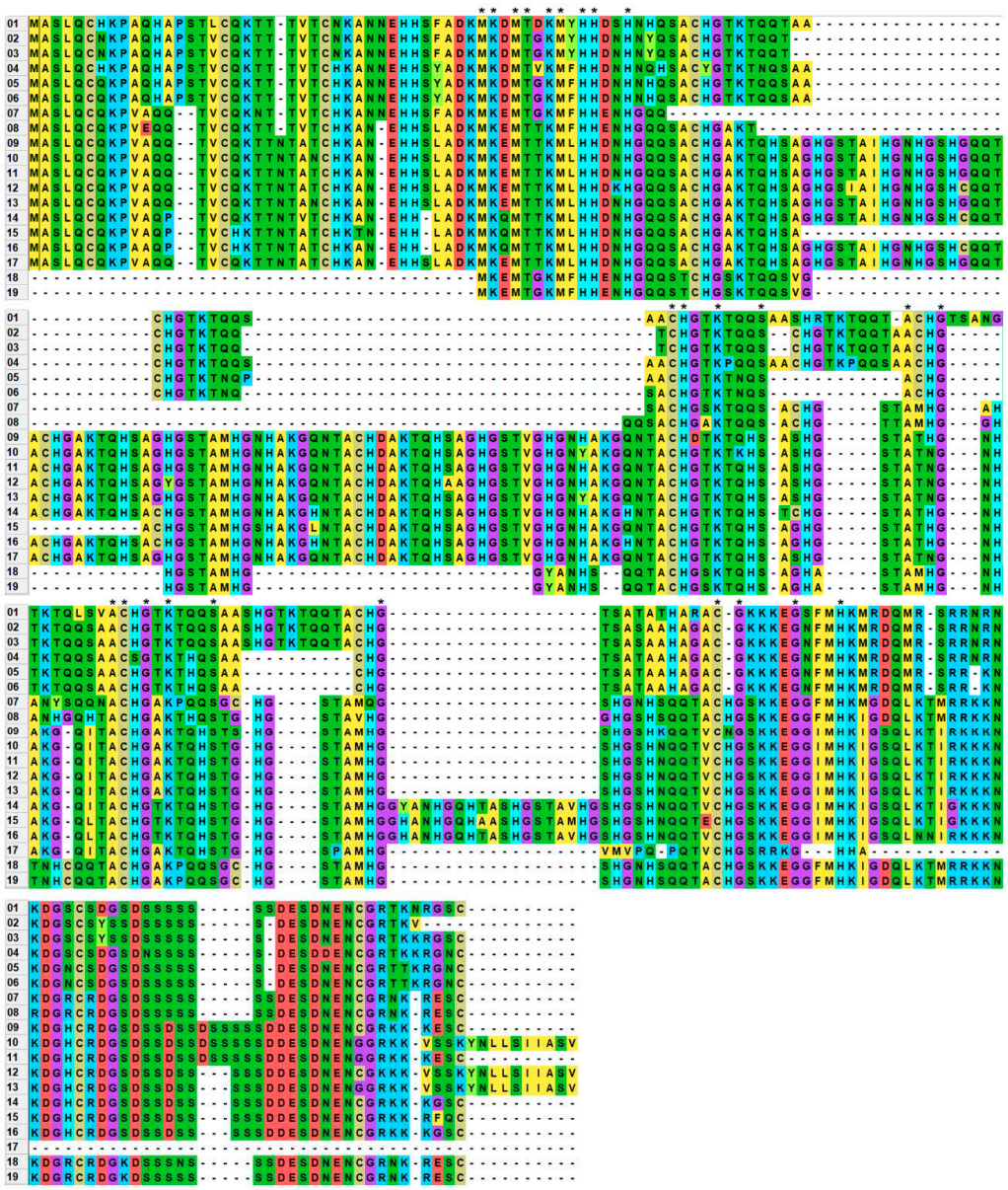

Figure 2. NbMIG21p sequence analysis. **(A)** NbMIG21p sequence. Five 7-aa long repeats are in bold. 11-aa stretches are underlined: color double lines mark perfect repeats, single or waived – imperfect. Letters in red – NLS predicted by LOCALIZER (https://localizer.csiro.au/); letters in a box – NoLS predicted using NOD http://www.compbio.dundee.ac.uk/www-nod/index.jsp. **(B)** Multiple alignment of MIG21p homologues from *Solanaceae* species performed using MEGA 11 software [30] with ClustalW algorithm. Asterisk indicates conservative residuals. 01 – NbMIG21 (ACY74744.2), 02 – *N. attenuata* hypothetical protein (OIT27799.1), 03 – *N. attenuata* uncharacterized protein (XP_019232815.1), 04 – *N. sylvestris* protein SSUH2 homolog (XP_009768095.1), 05 – *N. tabacum* uncharacterized protein (XP_016494112.1), 06 – *N. tomentosiformis* hornerin-like (XP_009592421.1), 07

 doi:10.20944/preprints202312.1011.v1

– *N. attenuata* uncharacterized protein (XP_019264939.1), 08 – *D. stramonium* hypothetical_protein (MCD7459440.1), 09 – *S. stenotomum* uncharacterized protein (XP_049376514.1), 10 – *S. verrucosum* hypothetical protein (WMV44005.1), 11 – *S. tuberosum* hornerin-like (XP_006343871.1), 12 – *S. commersonii* hypothetical protein (KAG5593335.1), 13 – *S. verrucosum* uncharacterized protein (XP_049361851.1), 14 – *S. lycopersicum* hornerin (XP_004245528.1), 15 – *S. chilense* hypothetical protein (TMW85354.1), 16 – *S. pennellii* hornerin-like (XP_015085049.1), 17 – *S. tuberosum* hypothetical protein (CAA12355.1), 18 – *N. tabacum* hornerin-like (XP_016480098.1), 19 – *N. sylvestris* hornerin-like (XP_009763094.1).

NbMIG21-encoded protein, NbMIG21p, contains five imperfect repeats of 11 amino acid (aa) residues (Figure 2A). NbMIG21p does not share any homology with annotated proteins in the UniProt database. Motif search service (https://www.genome.jp/tools/motif/) revealed that NbMIG21p fragment from 15 to 81 positions contains motif corresponding to ubinuclein conserved middle domain (PF14075) [31] (Figure S2). However, among predicted and putative proteins similar sequences were discovered in several *Solanaceae* species from genera *Nicotiana*, *Solanum*, *Datura* (Figure 2B). NbMIG21p C-terminal sequence contains multiple positively charged lysine and arginine residues, that are characteristic of nuclear localization signal (NLS). NbMIG21p analysis using bioinformatic tool for NLS prediction - LOCALIZER (https://localizer.csiro.au/) [32] revealed an NLS while nucleolus localization signal (NoLS) predictor - NOD (http://www.compbio.dundee.ac.uk/www-nod/index.jsp) [33,34] identified NoLS in NbMIG21p sequence.

2.2. NbMIG21p intracellular localization

To analyze NbMIG21p subcellular localization genetic constructs encoding NbMIG21p and GFP fuse were obtained: 35S-NbMIG21:GFP and 35S-GFP:NbMIG21. To exclude reporter protein position effect GFP was added to NbMIG21p as N-terminal or C-terminal fuse. Moreover, the construct encoding NbMIG21p fuse with RFP was also tested (Figure S3). All constructs were based on pCambia1300 backbone supplemented with additional 35S-promoter and terminator. *N. benthamiana* leaves were infiltrated with agrobacteria containing either 35S-NbMIG21:GFP, 35S-GFP:NbMIG21 or 35S-NbMIG21:RFP plasmid. 3 days after agroinfiltration confocal microscopy images of epidermal cells were obtained (Figure 3). GFP fluorescent signal was detected in the cytoplasm but the majority of the protein was localized to the nucleus with the highest intensity in some subnuclear structures that are likely correspond to nucleolus. The same localization was observed for NbMIG21:RFP (Figure S3).

Preprints (www.preprints.org) | NOT PEER-REVIEWED | Posted: 13 December 2023 doi:10.20944/preprints202312.1011.v1

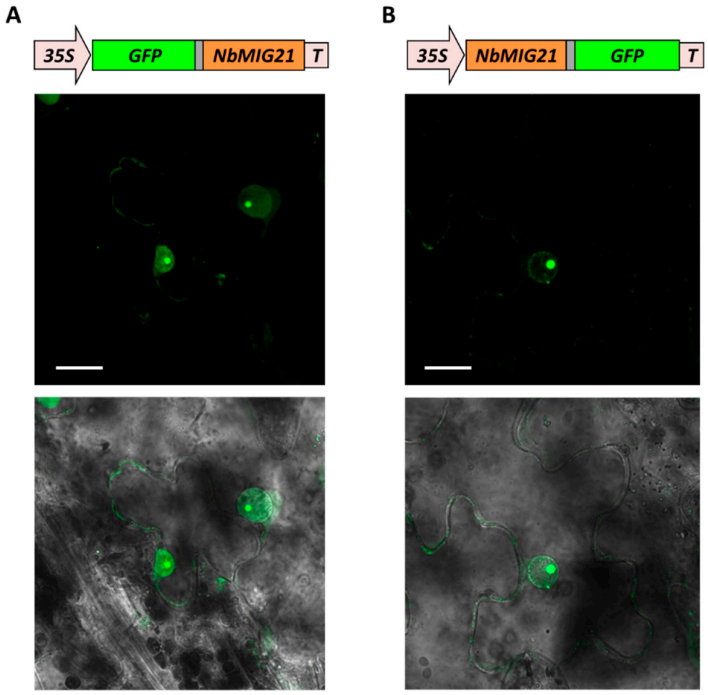

Figure 3. NbMIG21p intracellular localization. Images of 35S-GFP:NbMIG21 **(A)** or 35S-NbMIG21:GFP **(B)** expressing epidermal cells of *N. benthamiana* leaves 3 dpi obtained using confocal fluorescence microscopy. Projection of several confocal sections (left) superimposed on a bright field image of the same cell (right). Bars = 20 μm. 35S, Cauliflower mosaic virus 35S promoter; T, 35S terminator of transcription.

To further clarify the intranuclear localization of NbMIG21p we obtained constructs encoding fibrillarin 2 (NbFib2) and coilin (NbCoil) fused with GFP. Fibrillarin is generally regarded as nucleolus and Cajal bodies marker [35] and coilin is a major protein of Cajal bodies [36]. We co-infiltrated *N. benthamiana* leaves with agrobacterium containing 35S-NbFib2:GFP or 35S-NbCoil:GFP and agrobacterium with 35S-RFP:NbMIG21 plasmid. RFP-tagged NbMIG21p fluorescence partly overlapped with GFP-tagged NbFib2 and NbCoil indicating nucleolus and Cajal bodies localization (Figure 4).

Preprints (www.preprints.org) | NOT PEER-REVIEWED | Posted: 13 December 2023 doi:10.20944/preprints202312.1011.v1

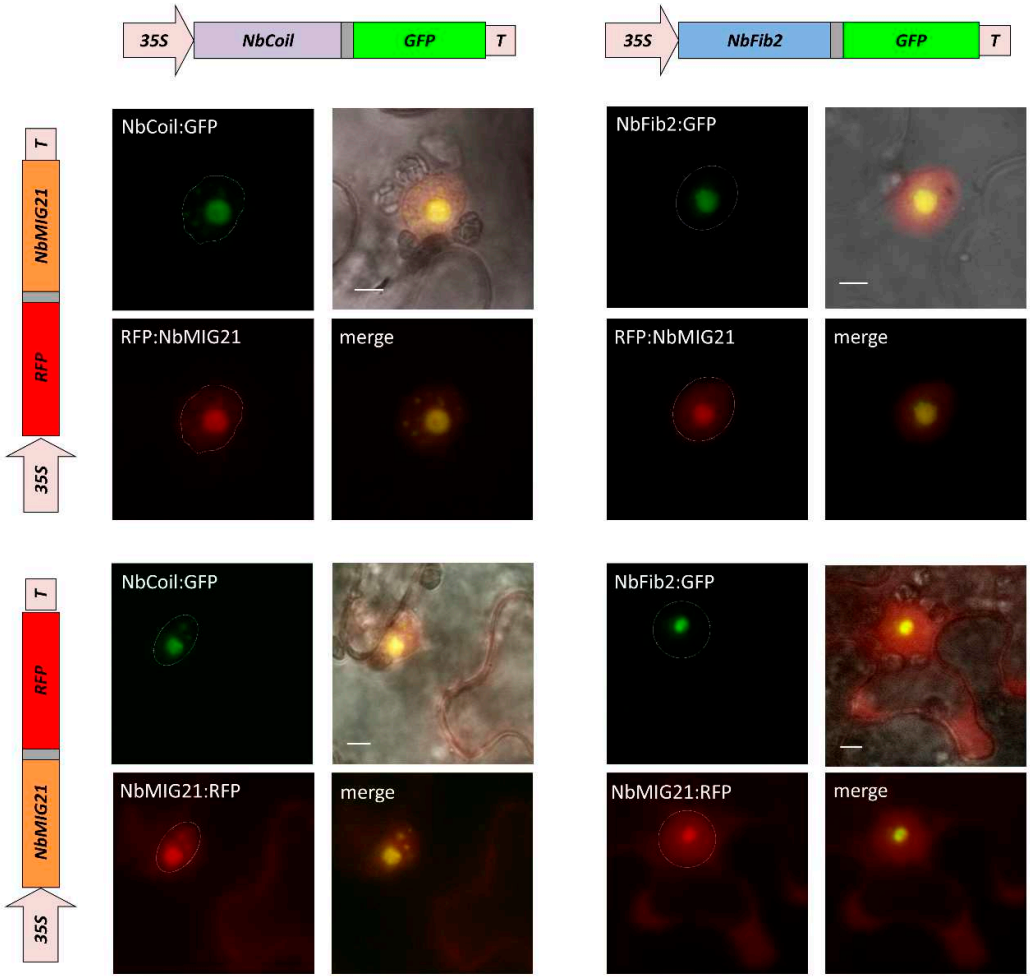

Figure 4. NbMIG21p co-localizes with fibrillarin and coilin. Schematic representation of genetic constructs encoding RFP-tagged NbMIG21p (left) and GFP-tagged fibrillarin or coilin (top). Fluorescent images of *N. benthamiana* cells 3 days after co-agroinfiltration with either 35S-NbMIG21:RFP or 35S-RFP:NbMIG21 and 35S-NbFib2:GFP or 35S-NbCoil:GFP. Nucleus is marked with a dashed line. Bar=5μm.

For NbMIG21 intracellular distribution analysis we also used bimolecular fluorescence complementation (BiFC) system, in which analyzed proteins are fused to non-fluorescent N- (YN) or C-terminal (YC) fragments of yellow fluorescent protein (YFP) and co-expressed in the same cell. If the proteins interact or are localized in a distance less than 100 Å, a recovery of YFP fluorescence is observed. We generated constructs encoding NbMIG21p, NbFib2 and NbCoil fused with either YN or YC fragments of YFP. Pairs of constructs containing NbMIG21 and NbFib2 or NbCoil sequence with corresponding YFP fragment were co-expressed in *N. benthamiana* leaves. At 3 dpi we observed YFP fluorescence for all pairs (Figure 5). For NbFib2:YN and NbMIG21:YC pair (or the opposite combination, NbFib2:YC and NbMIG21:YN, data not shown) fluorescence was detected mainly in the nucleolus (Figure 5A). For NbCoil:YC and NbMIG21:YN pair YFP fluorescence was distributed in multiple subnuclear structures that correspond to Cajal bodies (Figure 5B). An antiviral protein, *N. benthamiana* reversibly glycosylated protein 1 (NbRGP1) [37], was used as a negative control for BiFC assay.

Preprints (www.preprints.org) | NOT PEER-REVIEWED | Posted: 13 December 2023 doi:10.20944/preprints202312.1011.v1

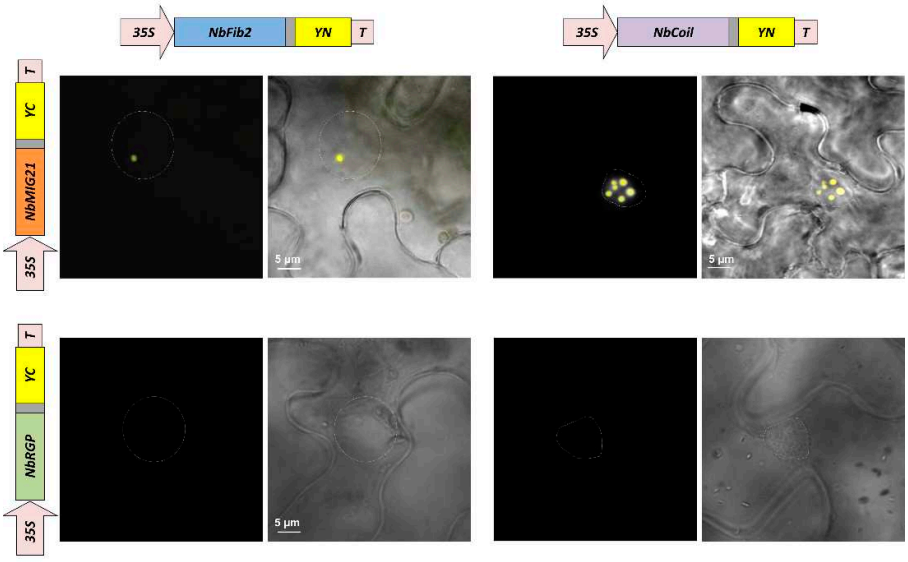

Figure 5. NbMIG21p co-localizes with fibrillarin and coilin. YFP fluorescence analyzed using fluorescent microscopy 3 days after infiltration of *N. benthamiana* leaves with pairs of agrobacteria containing plasmids for expression of 35S-NbMIG21:YN and 35S-NbFib2:YC (left), 35S-NbMIG21:YC and 35S-NbCoil:YN (right). For each pair fluorescence image and superimposed on visible light image are presented. 35S-NbRGP1:YC is used as a negative control. Nucleus is marked with a dashed line. Bar=5µm.

We concluded that NbMIG21p is distributed between nucleolus and Cajal bodies. Moreover, the obtained results could indicate NbMIG21p interactions with either NbFib2 or NbCoil.

2.3. Assessment of NbMIG21 influence on nucleocytoplasmic transport

NbMIG21 was initially identified among methanol-inducible genes and it shares some feature of these genes such as ability to stimulate intercellular transport of macromolecules and to facilitate tobacco mosaic virus reproduction [18]. Moreover, it has nuclear localization. Thus we suggested that it could affect nucleocytoplasmic transport as it was shown for PME [22] and for another MIG – NbAELP [21]. To assess the efficiency of nucleocytoplasmic transport we used GFP reporter fused to human prothymosin alpha NLS. Normally, GFP:NLS localizes to the nucleus but when co-expressed with NbMIG21, its distribution changes from nuclear to nucleocytoplasmic (Figure 6A). We quantified the percent of cells with GFP:NLS nucleocytoplasmic localization from total number of cells with GFP fluorescence: in areas infiltrated with 35S-NbMIG21 this ratio increased ~5-fold compared to the control area. In addition, *NbMIG21* overexpression leads to ~2-fold increase in the number of cells containing GFP:NLS compared to control. It could indicate either more efficient transformation or more active intercellular transport, due to which fluorescence is observed not only in transfected cells, but also in neighbouring cells, where GFP:NLS gets through plasmodesmata.

Preprints (www.preprints.org) | NOT PEER-REVIEWED | Posted: 13 December 2023 doi:10.20944/preprints202312.1011.v1

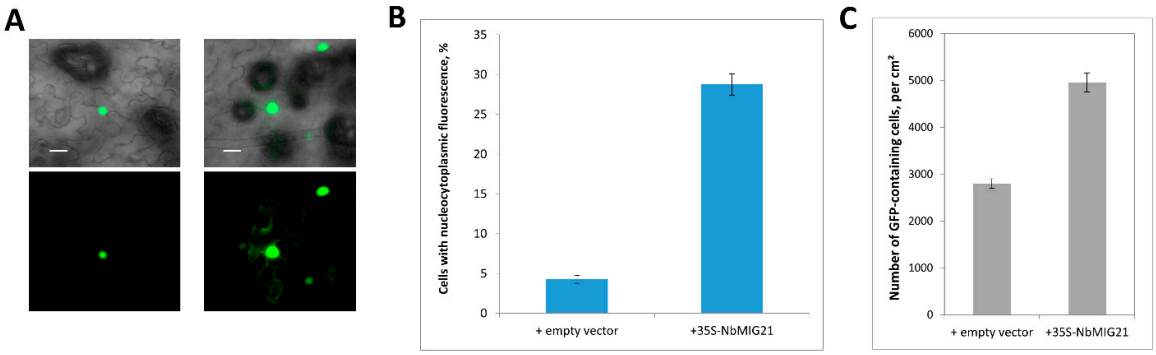

Figure 6. Increased expression of *NbMIG21* interferes with GFP:NLS nuclear import. **(A)** Representative images of nuclear (left) and nucleocytoplasmic (right) GFP:NLS distribution. Fluorescent image (lower panel) and overlay on bright-field image (upper panel). Bar = 20 μm. **(B)** Quantification of GFP:NLS subcellular localization 48 h after infiltration with 35S-GFP:NLS and 35S-NbMIG21 or "empty" vector. **(C)** Number of GFP:NLS-containing cells per square cm.

2.4. NbMIG21 facilitates viral intercellular transport

Earlier NbMIG21 was demonstrated to stimulate TMV-based GFP-encoding viral vector reproduction that was assessed by quantification of GFP fluorescence [18]. However, the observed increase in GFP accumulation could be both due to more efficient viral RNA synthesis and enhanced intercellular transport. To distinguish between these two processes here we assessed TMV:GFP cell-to-cell spread by measuring foci size as was performed earlier [38]. For this we used optimized dilution of TMV:GFP-containing agrobacterium suspension to obtain individual infected cells. We performed joint infiltration of *N. benthamiana* leaves with TMV:GFP and 35S-NbMIG21, while combination with "empty" vector was used as negative control. 5 days after infiltration we quantified the ratio of GFP-containing foci of different size (Figure 7A) and GFP fluorescence intensity (Figure S4).

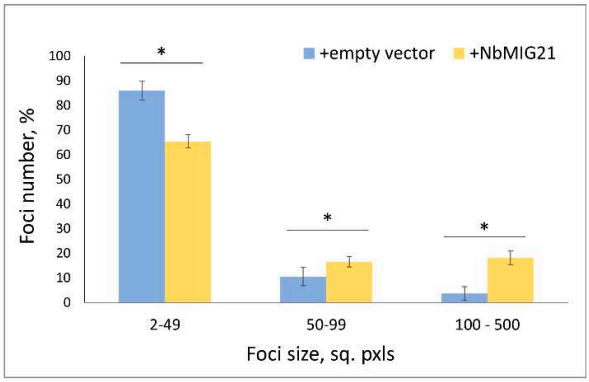

Figure 7. *NbMIG21* increased expression stimulates TMV:GFP intercellular transport. The percentage of TMV:GFP-expressing foci of different sizes quantified at 5th day after agroinfiltration of TMV:GFP and "empty" vector or 35S-NbMIG21. *, $p<0.05$ (Student's t-test).

The percentage of small foci (2-49 sq. pxls) decreased in areas with elevated *NbMIG21* expression while the number of larger foci (100-500 sq. pxls) increased there. The foci size reflects the efficiency of viral cell-to-cell movement. GFP fluorescence intensity shows viral vector-mediated GFP accumulation level. Thus, the obtained results indicate that TMV:GFP intercellular spread is more efficient in areas with increased *NbMIG21* expression.

Preprints (www.preprints.org) | NOT PEER-REVIEWED | Posted: 13 December 2023 doi:10.20944/preprints202312.1011.v1

2.5. NbMIG21 promoter identification and verification

Since *NbMIG21* mRNA level increases in response to gaseous methanol treatment [18] its regulation could occur at transcription level. We hypothesized that *NbMIG21* promoter could be methanol-sensitive. To check this assumption, we isolated a region of 1128 bp upstream of *NbMIG21* coding sequence from *N. benthamiana* genomic DNA. It completely corresponded to the reference genome scaffold available at https://solgenomics.net/organism/Nicotiana_benthamiana/genome. Bioinformatic analysis of the obtained sequence using PlantCARE tool (https://bioinformatics.psb.ugent.be/webtools/plantcare/html/) (Table S1) revealed elements involved in the response to light stress as well as motives related to recognition of abscisic and salicylic acids and auxin.

To verify the ability of the isolated sequence (designated PrMIG21) to serve as a promoter and to direct mRNA synthesis we generated a genetic construct PrMIG21-GFP containing *GFP* reporter gene downstream of the putative promoter. PrMIG21-GFP was delivered into cells of *N. benthamiana* leaves via agroinfiltration.

Infiltrated leaves on the third day after infiltration were examined under a fluorescence microscope. We observed GFP fluorescence at 3 dpi in the infiltrated leaves indicating that PrMIG21 is able to direct mRNA synthesis and thus possesses promotor activity (Figure 8).

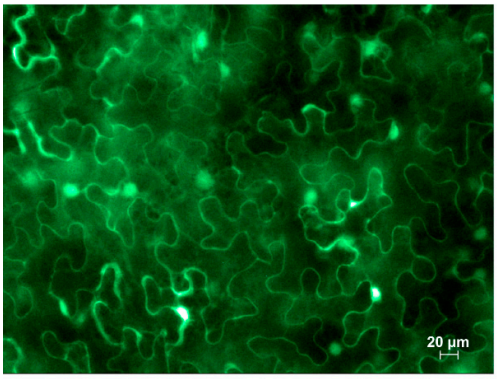

Figure 8. Fluorescent microscopy image of GFP accumulation in cytoplasm in leaves infiltrated with PrMIG21-GFP at 3 dpi. Mixture for infiltration was supplemented with agrobacteria containing plasmid for expression of p19 silencing suppressor of tomato bushy stunt virus.

2.6. PrMIG21 is methanol-sensitive

In order to assess if PrMIG21 is methanol-sensitive and evaluate the effect of gaseous methanol on the efficiency of PrMIG21-directed *GFP* mRNA accumulation, we treated plants with physiological concentration of methanol after infiltration and collected samples at different time points. The experimental set-up and workflow is presented in Figure 9A. Fully expanded *N. benthamiana* leaves were infiltrated with *Agrobacterium* suspensions containing PrMIG21-GFP construct. 24 hours post inoculation (hpi) leaf samples were collected with a hole punch and then one group of plants was placed for 24 h into the 20-l desiccator containing droplet of methanol on filter paper (200µl) to achieve gaseous methanol concentration comparable with physiological [18] and the other group (control) was incubated without methanol (Figure 9A). Then all plants were kept under normal greenhouse conditions for another 24 h. Samples were collected at the following time points: 27 hpi (3 h with methanol), 48 hpi (24 h in methanol), 72 hpi (24 h after methanol treatment). The relative amount of *GFP* mRNA was determined by qRT-PCR (Figure 9B).

Preprints (www.preprints.org) | NOT PEER-REVIEWED | Posted: 13 December 2023 doi:10.20944/preprints202312.1011.v1

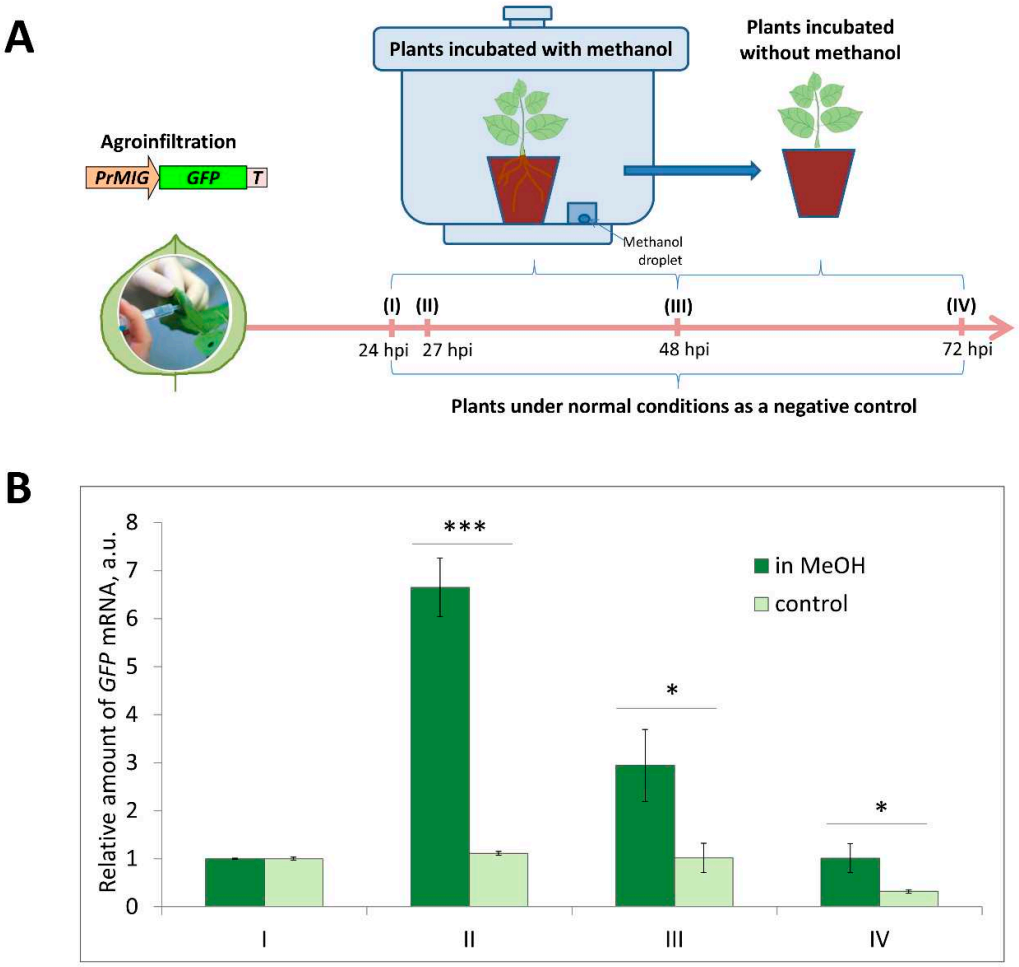

Figure 9. PrMIG21 is methanol-sensitive. **(A)** Schematic representation of experimental work flow with sample collecting time points indicated. **(B)** Relative amount of *GFP* mRNA in leaves of *N. benthamiana* plants agroinfiltrated with PrMIG21-GFP and treated with gaseous methanol. Amount of GFP mRNA at time point "I" is taken as 1. Student's t-test was applied to assess statistical significance of difference between control plants and plants incubated with methanol. *, $p<0.05$, ***, $p<0.001$.

Our results show that *GFP* mRNA level drastically increased after 3-h incubation with gaseous methanol with further decrease next time point (after 24-h methanol treatment) and recovering to the normal level after another 24 h under normal conditions. Thus, PrMIG21 is methanol-sensitive and is rapidly activated in response to gaseous methanol within first hours.

2.7. NbMIG21 interacts with promoter regions in vitro

The nuclear and nucleolus localization of NbMIG21 may indicate its potential ability to interact with nucleic acids. To test this assumption, we obtained recombinant 6xHis-MIG21 in *Escherichia coli* cells and performed *in vitro* binding of this protein with different promoter regions analyzing results by gel retardation assay (Figure 10). We used sequences of several available promoters of various *N. benthamiana* genes including PrKPILP [39], PrThio [40], PrNtPME and PrAELP [21], and identified here PrMIG21 as well as cauliflower mosaic virus 35S promoter, expecting that promoters contain common regulatory elements, which may be important for NbMIG21 binding.

Recombinant NbMIG21 was shown to interact both with plant gene promoters and a promoter from the phytovirus genome: NbMIG21 partly retains each tested DNA in the gel wells. Bovine serum albumin (BSA) and two recombinant plant proteins - *N. benthamiana* beta-1,3-glucanase (BG) [21] and

Preprints (www.preprints.org) | NOT PEER-REVIEWED | Posted: 13 December 2023 doi:10.20944/preprints202312.1011.v1

Arabidopsis thaliana Kunitz trypsin inhibitor (AtKTI) [42] – were used as negative controls. Noteworthy, best binding was observed for 35S-promoter which correlates with this promoter efficiency compared to other tested sequences.

Based on gel retardation assay results we concluded that NbMIG21 is able to bind DNA *in vitro*.

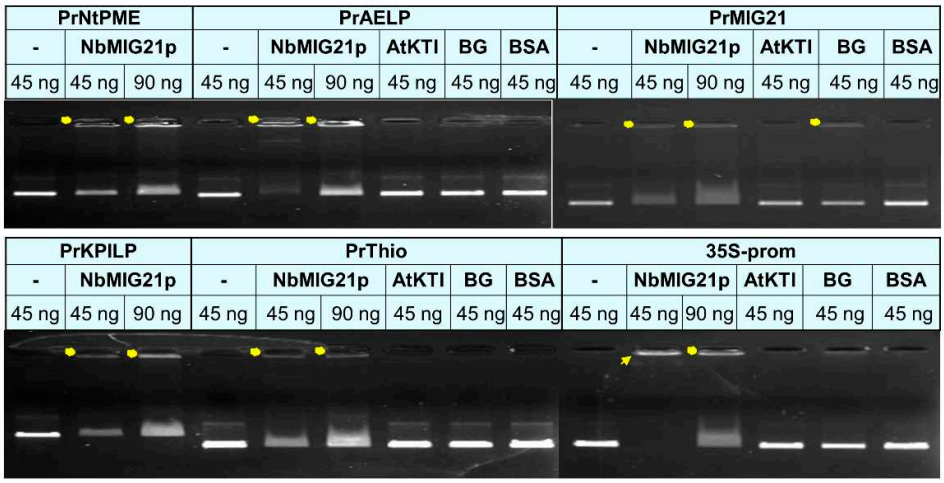

Figure 10. Gel retardation assay of PCR fragments representing promoter regions and 6xHis-NbMIG21. Two amounts of PCR fragments were used – 45 and 90 ng – as indicated above each lane. NbMIG21p and control proteins were used in a concentration of 200 ng. Yellow dots indicate retarded NbMIG21p-bound PCR fragments, arrow indicates fully bound PCR fragment of 35S promoter. AtKTI, *A. thaliana* Kunitz trypsin inhibitor (AtKTI); BG, *N. benthamiana* beta-1,3-glucanase; BSA, bovine serum albumin, were used as negative controls.

3. Discussion

Gaseous methanol was demonstrated to be a signal molecule that activates methanol-inducible genes (MIGs) expression. It was shown that both methanol treatment and increased expression of such MIGs as *BG*, *NbAELP* and *NbMIG21* stimulated intercellular transport of 2xGFP and TMV-based viral vector reproduction [18]. However, the mechanism of MIGs activation and functioning is still to be elucidated. Here we took a closer look at uncharacterized *NbMIG21* identified earlier as a gene expression of which increases in response to gaseous methanol. *NbMIG21*-encoded protein, NbMIG21p, is rich in glutamine residues, contains several amino acid repeats, predicted NLS and NoLS. We have found NbMIG21p homologues only among predicted proteins of *Solanaceae* species but not among annotated proteins. Noteworthy, all aligned sequences are rather conservative, they contain repeats and arginine/lysine- and serine-rich stretches the C-terminal part (Figure 2).

Analysis of NbMIG21p intracellular distribution revealed that it is indeed nucleus- and nucleolus-localized protein. It potentially interacts with the major nucleolus protein fibrillarin and Cajal bodies protein coilin as was shown in co-localization experiments and using BiFC system (Figure 5). Despite fibrillarin and coilin are regarded as markers of abovementioned subnuclear structures, they are also detected in other regions of the nucleus. For example, RFP-tagged fibrillarin localized both to the nucleolus and Cajal bodies, while overexpressed coilin fused with GFP was visualized in nucleoplasm, Cajal bodies and nucleolus [43]. Thus, based on co-localization studies we could conclude that NbMIG2p is distributed between nucleoplasm, nucleolus and Cajal bodies.

Previously it was shown that increased *NbMIG21* expression stimulates accumulation of GFP produced from TMV-based viral vector [18]. However, viral vector reproduction is the sum of replication, RNA stability and transport, and from the reported results it was unclear whether the obtained effect was due to the facilitation of transport or stimulation of viral RNA replication and accumulation. Here we have shown that *NbMIG21* increased expression induced activation of TMV:GFP local spread leading to formation of larger GFP-expressing infection foci (Figure 7). At the same time, GFP fluorescence intensity in the analyzed foci did not differ between experimental group

 doi:10.20944/preprints202312.1011.v1

and control (Figure S4) indicating comparable levels of vector-mediated GFP expression and accumulation. Thus, conditions favorable for viral infection are created mainly due to stimulation of intercellular transport and increased efficiency of viral local spread upon increased *NbMIG21* expression.

However, we could not exclude the impact of NbMIG21p effect on nucleocytoplasmic transport in stimulation of viral vector reproduction. It is known that plant viruses of different taxonomy groups (including viruses the lifecycle of which takes place in the cytoplasm) exploit nucleus of the host cell and interact with nuclear factors to facilitate infection [44]. Moreover, the same nuclear protein could play opposite role for different viruses – stimulating or suppressing it as was shown, for example, for coilin [43]. NbMIG21p interferes with nucleocytoplasmic transport similar to another MIG – NbAELP that was also demonstrated to impede GFP:NLS nuclear import [21] and stimulate viral vector reproduction [18]. PME, which is not a MIG but is a key player in methanol production, represents another example of the factor that prevents NLS-containing proteins from entering the nucleus in favor of viral infection: PME-induced inhibition of ALY nuclear import results in substantial increase in viral reproduction [22,45]. Thus, we suggested that one of the mechanisms of NbMIG21p-mediated facilitation of viral infection is realized via interference with nucleocytoplasmic transport.

Taking into account that the motif search engine (https://www.genome.jp/tools/motif/) revealed a motif resembling ubinuclein conserved middle domain in NbMIG21p sequence (Figure S2) we can speculate that NbMIG21p might be involved in chromatin reorganization processes caused by abiotic stress as was demonstrated for ubinucleins [46]. The online resource http://www.ebi.ac.uk/thornton-srv/databases/pdbsum/ found a list of various protein domains with rather low similarity to NbMIG21p but even though among them were nucleic acid-binding ones: Zinc finger Ran-binding domain-containing protein 2 (O95218) localized in nucleus [47] and ADP-ribosylation factor-like protein 6-interacting protein 4 (Q66PJ3) involved in modulating alternative pre-mRNA splicing also localized in nucleus and nucleolus [48]. Taken together NbMIG21p localization in nucleus and nucleolus could indicate nucleic acids binding properties. Indeed, NbMIG21p was shown to be able to bind nucleic acids, in particular DNA as was demonstrated *in vitro* in gel retardation assay. We tested promoter regions and revealed the most efficient binding for the 35S-promoter of Cauliflower mosaic virus (Figure 10) which is the "strongest" of all assessed sequences (i.e. provides the highest level of mRNA accumulation). Such DNA-binding property could indicate that NbMIG21p participates in regulation of intercellular transport affecting genes expression. Nucleic acid binding proteins are crucial for various biological processes, including replication, transcription, and translation [49]. Among these proteins are transcription factors, chromatin remodelers, and RNA-binding proteins, etc. The regulation of their genes involves complex mechanisms that control their expression at the transcriptional and post-transcriptional levels. Various regulatory elements, such as enhancers, promoters, and transcription factor binding sites, modulate the expression of these genes. Inducible promoters are often found in genes that need to be turned on or off rapidly in response to changes in the cellular environment [50]. Inducible promoters allow dynamic control of gene expression, enabling cells to adapt to various internal and external cues, including stress, developmental signals, or environmental changes. The activators of such promoters are often small molecules or proteins. We obtained and characterized *NbMIG21* promoter, which was experimentally confirmed to be activated in response to gaseous methanol. PrMIG21-mediated *GFP* mRNA accumulation significantly increased after 3-h incubation with gaseous methanol and started to decrease but still was elevated after 24-h methanol treatment (Figure 9). This is in line with previously obtained results on endogenous *NbMIG21* expression: earlier it was shown that *NbMIG21* mRNA level increased after 3-h incubation in desiccator with methanol vapors and peak after 21-h of further plants incubation in normal conditions [18]. According to bioinformatic analysis PrMIG21 contains various regulatory elements including stress-responsive and hormone-sensitive (Table S1). Methanol could act directly on some unidentified sequence in PrMIG21 or indirectly via known transcription factors, however, this is the subject of further studies.

 doi:10.20944/preprints202312.1011.v1

Collectively, our results on *NbMIG21* properties and functions indicate that it is one of key players that is responsible for manifestation of methanol-induced response of the plant cell. Here we focused on *NbMIG21* effect towards viral infection, however, the other important aspect of methanol action is induction of antibacterial resistance. *NbMIG21* involvement in it could be exhibited at the level of nucleocytoplasmic transport control and gene expression regulation. It is known, that bacterial pathogens exploit host cell nucleus during colonization, they possess special proteins – nucleomodulins – that can enter the nucleus and affect host gene expression interfering with plant immune response thus facilitating bacterial reproduction [51]. Methanol-induced susceptibility to the viral infection is the reverse side of acquired resistance to bacteria. And it is not the only example of balancing between resistance and susceptibility: recently it was shown that increased production of NLS-containing proteins (as a mimetic of nucleomodulins) in plant cell leads to the induction of γ-thionin, a factor of antibacterial defense response, but the side effect of this cellular reaction is sensitivity to the virus – viral vector reproduction is stimulated both upon γ-thionin elevated expression or massive synthesis of foreign NLS-containing proteins. The exact mechanism of these effects is unknown but likely it involves interference with nucleocytoplasmic transport [40].

Therefore, the potential role of *NbMIG21* in resistance to bacterial pathogens and the mechanism of NbMIG21p functioning are the subject of further studies as well as the properties of other MIGs.

4. Materials and Methods

4.1. Plant growth conditions

Wild type *Nicotiana benthamiana* plants were grown in pots with a mixture of leafy soil, humus, peat and sand under standard conditions in a temperature-controlled greenhouse at 25/18℃ with a day/night cycle of 16/8 hours. The 6-7-week-old plants with 5-6 true leaves were used in the experiments unless otherwise specified.

4.2. Agroinfiltration

Agrobacterium tumefaciens (strain GV-3101) was grown at 28° on LB medium with appropriate antibiotics (50μg/mL rifampicin, 25μg/mL gentamicin and 50μg/mL kanamycin or carbenicillin depending on the plasmid). Agroinfiltration buffer containing 10 mM MES (pH 5.5) and 10 mM MgCl2 was added to an aliquot of an overnight culture of *A. tumefaciens* to dilute it to the OD_{600} 0.1 or 0.005 for TMV:GFP experiment. Mixtures for infiltration except TMV:GFP and GFP-NLS experiments were supplemented with agrobacteria containing plasmid for expression of p19 silencing suppressor of Tomato bushy stunt virus. Leaves of *N. benthamiana* plants were infiltrated with agrobacterium suspension using a syringe without needle.

4.3. Whole plant methanol treatment

Fully expanded leaves of *N. benthamiana* were infiltrated with agrobacterium containing PrMIG21-GFP plasmid. 24 hours post inoculation (hpi), samples were collected using a hole punch, and three plants were placed into a 20-l desiccator that contained a droplet of methanol on filter paper (200μl) and sealed for 24 hours, while the remaining three plants were maintained under standard conditions. Subsequently, all plants were kept without methanol for an additional 24 hours. Samples from leaves were collected in several time points: 24, 27, 48 and 72 hpi.

4.4. GFP, RFP and YFP Imaging

GFP fluorescence in the infected leaves was observed under a handheld UV source. TMV:GFP foci were analyzed 5 days post inoculation (dpi). GFP and YFP fluorescence was visualized using an AxioVert 200M microscope (Carl Zeiss, Jena, Germany) equipped with an AxioCam MRc digital camera. The excitation/detection wavelength (i) for GFP and YFP was 487/525 nm; for RFP – 561/625 nm, respectively. Confocal microscopy was performed using a Nikon C2 confocal laser scanning microscope. The intracellular distribution of fluorescent proteins was observed 72 hours after

 doi:10.20944/preprints202312.1011.v1

infiltration. TMV:GFP foci area and fluorescence intensity were measured using open-source ImageJ software [52].

4.5. Genomic DNA Extraction

Genomic DNA was extracted from frozen in liquid nitrogen *N. benthamiana* leaves using the Diatom DNA Prep kit as per the manufacturer's protocol (Galart-Diagnosticum, Moscow, Russia).

4.6. RNA Extraction and cDNA Synthesis

Total RNA was extracted from plant tissues using TriReagent (MRC, Houston, TX, USA). The RNA concentration was determined using a Nanodrop ND-1000 spectrophotometer (Isogen Life Sciences, Utrecht, The Netherlands). First-strand cDNA was synthesized using random hexamers, oligo-dT primer, and Superscript II reverse transcriptase (Thermo Fisher Scientific, Waltham, MA, USA).

4.7. Quantitative Real-Time PCR (qRT-PCR)

Quantitative real-time PCR was performed using the iCycler iQ real-time PCR detection system (Bio-Rad, Hercules, CA, USA). Target genes were amplified using specific primers and Eva Green master mix (Syntol, Moscow, Russia), while reference genes were amplified using primers to the 18S rRNA gene and the protein phosphatase 2A gene (PP2A) (Table S2). Each sample was run in triplicate, and a non-template control was included. At least five biological replicates were performed, and the qRT-PCR results were analyzed using the Pfaffl algorithm [53].

4.8. Plasmid Constructs

To obtain NbMIG21 coding sequence PCR using *N. benthamiana* cDNA as a template with following primers "N-NbMIG21-*Acc65*I_f"/"C-NbMIG21-*Sal*I_r" was performed and PCR product was cloned into pAL2-T plasmid (Evrogen, Moscow, Russia). To obtain a set of constructs encoding NbMIG21 fusions with various fluorescent protein: 35S-NbMIG21:GFP, 35S-NbMIG21:RFP, 35S-NbMIG21:YC and NbMIG21:YN, a fragment encoding NbMIG21 without a stop codon and flanked by Acc65I/BamHI recognition sites was synthesized using "N-NbMIG21-*Acc65*I_f"/"N-NbMIG21-*BamH*I_r" pair of primers. This fragment was digested with Acc65I/BamHI and inserted into pCambia-35S vector containing either GFP-, RFP-, YN- or YC-encoding sequence without start codon [37] using the same sites.

To obtain 35S-GFP:NbMIG21, 35S-YN:NbMIG21 and 35S-YC:NbMIG21 plasmids NbMIG21 fragment without start codon was synthesized using "C-NbMIG21-*BamH*I_f"/"C-NbMIG21-*Sal*I_r" pair of primers. Corresponding fluorescent tag-encoding sequence without stop codon was amplified using "GFP-*Acc65*I_f"/"GFP-*BamH*I_r", "YN-*Acc65*I_f"/"YN-*BamH*I_r", "YC-*Acc65*I_f"/"YC-*BamH*I_r" pair of primers, respectively. NbMIG21 fragment was digested with *BamH*I/*Sal*I, GFP, YN and YC fragments were digested with *Acc65*I/*BamH*I. Each fragment encoding the corresponding fluorescent tag together with NbMIG21 fragment was ligated into modified pCambia-35S vector digested with *Acc65*I/*Sal*I enzymes.

Sequences encoding coilin (NbCoil, GeneBank accession number MK903618.1) and fibrillarin (NbFib2, GeneBank accession number AM269909.1) without a stop codon were amplified from *N. benthamiana* cDNA using the "NbCoilin-*Acc65*I_f"/"NbCoilin-*BamH*I_r" and "NbFib2-*Acc65*I_f"/"NbFib2-*BamH*I_r" primer pairs. The algorithm for obtaining 35S-NbCoil:GFP, 35S-NbCoil:YN, 35S-NbCoil:YN and 35S-NbFib2:GFP, 35S-NbFib2:YN, 35S-NbFib2:YC was the same as for NbMIG21-encoding constructs.

To obtain a plasmid for NbMIG21 recombinant protein production in *Escherichia coli* cells, NbMIG21-encoding fragment without a start codon was obtained with the "6H-NbMIG21-*Acc65*I_f"/"C-NbMIG21-*Sal*I_r" primer pair and Acc65I and SalI recognition sites at the ends of the resulting fragment. The PCR product was digested with the Acc65I-SalI restriction enzymes and

cloned into the pQE-30 vector (QIAGEN, Netherlands) digested with Acc65I/SalI. Therefore, 6xHis-NbMIG21 was obtained.

4.9. Production of recombinant MIG21 protein

NbMIG21 with N-terminal hexahistidine tag (6xHis) was obtained according to the protocol outlined in The QIAexpressionist™ handbook. *E. coli* (strain SG13009) was used for accumulation of the recombinant protein. 6xHis-NbMIG21 purification was performed using immobilized-metal affinity chromatography on Ni-NTA agarose resin. Eluted from Ni-NTA column 6xHis-NbMIG21 was analyzed by SDS PAAG electrophoresis and dialyzed using a dialysis tubing (Spectrum Laboratories Specpor 4, 12-14K MWCO). The initial dialysis buffer contained 10 mM Tris-HCl (pH 4.5), 2 M urea and 80 mM NaH_2PO_4 with a stepwise reduction of urea and NaH_2PO_4 content. Dialysis was performed for 2 hours in each buffer and overnight incubation in the final buffer (10 mM Tris-HCl (pH 4.5) and 20 mM NaH_2PO_4) at +4°C. Further samples were concentrated using Sephadex dry powder.

4.10. In vitro DNA binding and gel retardation assay

200 ng of dialyzed recombinant 6xHis-MIG21 was added to 45 or 90 ng of DNA fragments corresponding to each of the tested promoter sequences. Binding was performed in the buffer containing 20 mM Tris-HCl pH 7.5, 1 mM DTT, 3 mM $MgCl_2$, 50 mM NaCl, for 1 h on ice. Bovine serum albumin, recombinant *A. thaliana* Kunitz trypsin inhibitor (AtKTI) and *N. benthamiana* 1,3-beta-glucanase (BG) were used as negative controls. Samples were then loaded to 1% agarose gel containing ethidium bromide and electrophoretic analysis was performed.

4.11. Statistical Analysis

Statistical analysis involved the use of Student's t-test. The y-axis error bars in all histograms represent the standard error of the mean values.

Supplementary Materials: The following supporting information can be downloaded at the website of this paper posted on Preprints.org. Figure S1: *NbMIG21* pattern of expression according to Version 6 Gene expression Atlas; Figure S2: NbMIB21p motif search; Figure S3: NbMIG21p:RFP intracellular localization; Figure S4: Relative intensity of GFP fluorescence in the analyzed TMV:GFP-expressing foci. Table S1: PrMIG21 cis-acting elements analysis; Table S2: Oligonucleotides used for qRT-PCR and cloning.

Author Contributions: Conceptualization, E.S. and T.K.; investigation, E.S., K.K. N.E.; writing—original draft preparation, E.S., K.K., T.K.; writing—review and editing, E.S., K.K. N.E., T.K.; visualization, N.E.; supervision, T.K.; project administration, E.S.; funding acquisition, E.S. All authors have read and agreed to the published version of the manuscript.

Funding: This research was funded by Russian Science Foundation, grant number 22-24-00895.

Institutional Review Board Statement: Not applicable.

Informed Consent Statement: Not applicable.

Acknowledgments: The authors thank Irina Savchenko for technical assistance, and acknowledge Lomonosov Moscow State University Development Program PNR5.13 for access to the scientific instruments.

Conflicts of Interest: The authors declare no conflict of interest. The funders had no role in the design of the study; in the collection, analyses, or interpretation of data; in the writing of the manuscript, or in the decision to publish the results.

References

1. Ramegowda, V.; Senthil-Kumar, M. The Interactive Effects of Simultaneous Biotic and Abiotic Stresses on Plants: Mechanistic Understanding from Drought and Pathogen Combination. *J. Plant Physiol.* **2015**, *176*, 47–54, doi:10.1016/j.jplph.2014.11.008.
2. Ganusova, E.E.; Burch-Smith, T.M. Review: Plant-Pathogen Interactions through the Plasmodesma Prism. *Plant Sci. Int. J. Exp. Plant Biol.* **2019**, *279*, 70–80, doi:10.1016/j.plantsci.2018.05.017.

3. Dorokhov, Y.L.; Ershova, N.M.; Sheshukova, E.V.; Komarova, T.V. Plasmodesmata Conductivity Regulation: A Mechanistic Model. *Plants* **2019**, *8*, 595, doi:10.3390/plants8120595.
4. Azim, M.F.; Burch-Smith, T.M. Organelles-Nucleus-Plasmodesmata Signaling (ONPS): An Update on Its Roles in Plant Physiology, Metabolism and Stress Responses. *Curr. Opin. Plant Biol.* **2020**, *58*, 48–59, doi:10.1016/j.pbi.2020.09.005.
5. Li, Z.P.; Paterlini, A.; Glavier, M.; Bayer, E.M. Intercellular Trafficking via Plasmodesmata: Molecular Layers of Complexity. *Cell. Mol. Life Sci.* **2021**, *78*, 799–816, doi:10.1007/s00018-020-03622-8.
6. Baldwin, I.T. Plant Volatiles. *Curr. Biol. CB* **2010**, *20*, R392-397, doi:10.1016/j.cub.2010.02.052.
7. Holopainen, J.K.; Blande, J.D. Molecular Plant Volatile Communication. *Adv. Exp. Med. Biol.* **2012**, *739*, 17–31, doi:10.1007/978-1-4614-1704-0_2.
8. Pichersky, E.; Noel, J.P.; Dudareva, N. Biosynthesis of Plant Volatiles: Nature's Diversity and Ingenuity. *Science* **2006**, *311*, 808–811, doi:10.1126/science.1118510.
9. Pelloux, J.; Rustérucci, C.; Mellerowicz, E.J. New Insights into Pectin Methylesterase Structure and Function. *Trends Plant Sci.* **2007**, *12*, 267–277, doi:10.1016/j.tplants.2007.04.001.
10. Jolie, R.P.; Duvetter, T.; Van Loey, A.M.; Hendrickx, M.E. Pectin Methylesterase and Its Proteinaceous Inhibitor: A Review. *Carbohydr. Res.* **2010**, *345*, 2583–2595, doi:10.1016/j.carres.2010.10.002.
11. Fall, R.; Benson, A.A. Leaf Methanol—the Simplest Natural Product from Plants. *Trends Plant Sci.* **1996**, *1*, 296–301.
12. Nemecek-Marshall, M.; MacDonald, R.C.; Franzen, J.J.; Wojciechowski, C.L.; Fall, R. Methanol Emission from Leaves (Enzymatic Detection of Gas-Phase Methanol and Relation of Methanol Fluxes to Stomatal Conductance and Leaf Development). *Plant Physiol.* **1995**, *108*, 1359–1368, doi:10.1104/pp.108.4.1359.
13. Komarova, T.V.; Sheshukova, E.V.; Dorokhov, Y.L. Cell Wall Methanol as a Signal in Plant Immunity. *Front. Plant Sci.* **2014**, *5*, 101, doi:10.3389/fpls.2014.00101.
14. Körner, E.; von Dahl, C.C.; Bonaventure, G.; Baldwin, I.T. Pectin Methylesterase NaPME1 Contributes to the Emission of Methanol during Insect Herbivory and to the Elicitation of Defence Responses in Nicotiana Attenuata. *J. Exp. Bot.* **2009**, *60*, 2631–2640, doi:10.1093/jxb/erp106.
15. von Dahl, C.C.; Hävecker, M.; Schlögl, R.; Baldwin, I.T. Caterpillar-Elicited Methanol Emission: A New Signal in Plant-Herbivore Interactions? *Plant J. Cell Mol. Biol.* **2006**, *46*, 948–960, doi:10.1111/j.1365-313X.2006.02760.x.
16. Dixit, S.; Upadhyay, S.K.; Singh, H.; Sidhu, O.P.; Verma, P.C.; K, C. Enhanced Methanol Production in Plants Provides Broad Spectrum Insect Resistance. *PloS One* **2013**, *8*, e79664, doi:10.1371/journal.pone.0079664.
17. Dixit, S.; Chandrashekar, K.; Upadhyay, S.K.; Verma, P.C. Transcriptional Plasticity and Cell Wall Characterization in High-Methanol-Producing Transgenic Tobacco Plants. *Agriculture* **2023**, *13*, 521, doi:10.3390/agriculture13030521.
18. Dorokhov, Y.L.; Komarova, T.V.; Petrunia, I.V.; Frolova, O.Y.; Pozdyshev, D.V.; Gleba, Y.Y. Airborne Signals from a Wounded Leaf Facilitate Viral Spreading and Induce Antibacterial Resistance in Neighboring Plants. *PLoS Pathog.* **2012**, *8*, e1002640, doi:10.1371/journal.ppat.1002640.
19. Srivastava, A.; Jain, G.; Sushmita; Chandra, S.; Kalia, V.; Upadhyay, S.K.; Dubey, R.S.; Verma, P.C. Failure of Methanol Detoxification in Pests Confers Broad Spectrum Insect Resistance in PME Overexpressing Transgenic Cotton. *Plant Sci.* **2023**, *333*, 111737, doi:10.1016/j.plantsci.2023.111737.
20. Dorokhov, Y.L.; Sheshukova, E.V.; Komarova, T.V. Methanol in Plant Life. *Front. Plant Sci.* **2018**, *9*.
21. Sheshukova, E.V.; Komarova, T.V.; Pozdyshev, D.V.; Ershova, N.M.; Shindyapina, A.V.; Tashlitsky, V.N.; Sheval, E.V.; Dorokhov, Y.L. The Intergenic Interplay between Aldose 1-Epimerase-Like Protein and Pectin Methylesterase in Abiotic and Biotic Stress Control. *Front. Plant Sci.* **2017**, *8*.
22. Komarova, T.V.; Citovsky, V.; Dorokhov, Y.L. Pectin Methylesterase Enhances Tomato Bushy Stunt Virus P19 RNA Silencing Suppressor Effects. In *RNAi Technology*; CRC Press, 2011; pp. 125–134 ISBN 978-1-57808-716-7.
23. German, L.; Yeshvekar, R.; Benitez-Alfonso, Y. Callose Metabolism and the Regulation of Cell Walls and Plasmodesmata during Plant Mutualistic and Pathogenic Interactions. *Plant Cell Environ.* **2023**, *46*, 391–404, doi:10.1111/pce.14510.
24. Fernandez-Calvino, L.; Faulkner, C.; Walshaw, J.; Saalbach, G.; Bayer, E.; Benitez-Alfonso, Y.; Maule, A. Arabidopsis Plasmodesmal Proteome. *PLOS ONE* **2011**, *6*, e18880, doi:10.1371/journal.pone.0018880.
25. Grison, M.S.; Brocard, L.; Fouillen, L.; Nicolas, W.; Wewer, V.; Dörmann, P.; Nacir, H.; Benitez-Alfonso, Y.; Claverol, S.; Germain, V.; et al. Specific Membrane Lipid Composition Is Important for Plasmodesmata Function in Arabidopsis. *Plant Cell* **2015**, *27*, 1228–1250, doi:10.1105/tpc.114.135731.
26. Pankratenko, A.V.; Atabekova, A.K.; Morozov, S.Y.; Solovyev, A.G. Membrane Contacts in Plasmodesmata: Structural Components and Their Functions. *Biochem. Mosc.* **2020**, *85*, 531–544, doi:10.1134/S0006297920050028.

27. Han, X.; Huang, L.-J.; Feng, D.; Jiang, W.; Miu, W.; Li, N. Plasmodesmata-Related Structural and Functional Proteins: The Long Sought-After Secrets of a Cytoplasmic Channel in Plant Cell Walls. *Int. J. Mol. Sci.* **2019**, *20*, 2946, doi:10.3390/ijms20122946.
28. Brunkard, J.O.; Runkel, A.M.; Zambryski, P.C. Plasmodesmata Dynamics Are Coordinated by Intracellular Signaling Pathways. *Curr. Opin. Plant Biol.* **2013**, *16*, 10.1016/j.pbi.2013.07.007, doi:10.1016/j.pbi.2013.07.007.
29. Stonebloom, S.; Brunkard, J.O.; Cheung, A.C.; Jiang, K.; Feldman, L.; Zambryski, P. Redox States of Plastids and Mitochondria Differentially Regulate Intercellular Transport via Plasmodesmata. *Plant Physiol.* **2012**, *158*, 190, doi:10.1104/pp.111.186130.
30. Tamura, K.; Stecher, G.; Kumar, S. MEGA11: Molecular Evolutionary Genetics Analysis Version 11. *Mol. Biol. Evol.* **2021**, *38*, 3022–3027, doi:10.1093/molbev/msab120.
31. Jarnot, P.; Ziemska-Legiecka, J.; Dobson, L.; Merski, M.; Mier, P.; Andrade-Navarro, M.A.; Hancock, J.M.; Dosztányi, Z.; Paladin, L.; Necci, M.; et al. PlaToLoCo: The First Web Meta-Server for Visualization and Annotation of Low Complexity Regions in Proteins. *Nucleic Acids Res.* **2020**, *48*, W77–W84, doi:10.1093/nar/gkaa339.
32. Sperschneider, J.; Catanzariti, A.-M.; DeBoer, K.; Petre, B.; Gardiner, D.M.; Singh, K.B.; Dodds, P.N.; Taylor, J.M. LOCALIZER: Subcellular Localization Prediction of Both Plant and Effector Proteins in the Plant Cell. *Sci. Rep.* **2017**, *7*, 44598, doi:10.1038/srep44598.
33. Scott, M.S.; Boisvert, F.-M.; McDowall, M.D.; Lamond, A.I.; Barton, G.J. Characterization and Prediction of Protein Nucleolar Localization Sequences. *Nucleic Acids Res.* **2010**, *38*, 7388–7399, doi:10.1093/nar/gkq653.
34. Scott, M.S.; Troshin, P.V.; Barton, G.J. NoD: A Nucleolar Localization Sequence Detector for Eukaryotic and Viral Proteins. *BMC Bioinformatics* **2011**, *12*, 317, doi:10.1186/1471-2105-12-317.
35. Zheng, L.; Yao, J.; Gao, F.; Chen, L.; Zhang, C.; Lian, L.; Xie, L.; Wu, Z.; Xie, L. The Subcellular Localization and Functional Analysis of Fibrillarin2, a Nucleolar Protein in Nicotiana Benthamiana. *BioMed Res. Int.* **2016**, *2016*, 2831287, doi:10.1155/2016/2831287.
36. Taliansky, M.E.; Love, A.J.; Kołowerzo-Lubnau, A.; Smoliński, D.J. Cajal Bodies: Evolutionarily Conserved Nuclear Biomolecular Condensates with Properties Unique to Plants. *Plant Cell* **2023**, *35*, 3214–3235, doi:10.1093/plcell/koad140.
37. Kamarova, K.A.; Ershova, N.M.; Sheshukova, E.V.; Arifulin, E.A.; Ovsiannikova, N.L.; Antimonova, A.A.; Kudriashov, A.A.; Komarova, T.V. Nicotiana Benthamiana Class 1 Reversibly Glycosylated Polypeptides Suppress Tobacco Mosaic Virus Infection. *Int. J. Mol. Sci.* **2023**, *24*, 12843, doi:10.3390/ijms241612843.
38. Ershova, N.; Kamarova, K.; Sheshukova, E.; Antimonova, A.; Komarova, T. A Novel Cellular Factor of Nicotiana Benthamiana Susceptibility to Tobamovirus Infection. *Front. Plant Sci.* **2023**, *14*.
39. Sheshukova, E.V.; Komarova, T.V.; Ershova, N.M.; Bronstein, A.M.; Dorokhov, Y.L. The Expression of Matryoshka Gene Encoding a Homologue of Kunitz Peptidase Inhibitor Is Regulated Both at the Level of Transcription and Translation. *Biochem. Mosc.* **2018**, *83*, 1255–1262, doi:10.1134/S0006297918100103.
40. Sheshukova, E.V.; Ershova, N.M.; Lipskerov, F.A.; Komarova, T.V. Enhanced Synthesis of Foreign Nuclear Protein Stimulates Viral Reproduction via the Induction of γ-Thionin Expression. *Plants* **2022**, *11*, 1530, doi:10.3390/plants11121530.
41. Sheshukova, E.; Komarova, T.V.; Pozdyshev, D.V.; Ershova, N.M.; Shindyapina, A.V.; Tashlitsky, V.N.; Sheval, E.V.; Dorokhov, Y.L. The Intergenic Interplay between Aldose 1-Epimerase-like Protein and Pectin Methylesterase in Abiotic and Biotic Stress Control. *Front. Plant Sci.* **2017**, *8*, doi:10.3389/fpls.2017.01646.
42. Sheshukova, E.V.; Komarova, T.V.; Ershova, N.M.; Shindyapina, A.V.; Dorokhov, Y.L. An Alternative Nested Reading Frame May Participate in the Stress-Dependent Expression of a Plant Gene. *Front. Plant Sci.* **2017**, *8*, 2137, doi:10.3389/fpls.2017.02137.
43. Shaw, J.; Love, A.J.; Makarova, S.S.; Kalinina, N.O.; Harrison, B.D.; Taliansky, M.E. Coilin, the Signature Protein of Cajal Bodies, Differentially Modulates the Interactions of Plants with Viruses in Widely Different Taxa. *Nucleus* **2014**, *5*, 85–94, doi:10.4161/nucl.28315.
44. Taliansky, M.E.; Brown, J.W.S.; Rajamäki, M.L.; Valkonen, J.P.T.; Kalinina, N.O. Involvement of the Plant Nucleolus in Virus and Viroid Infections. *Adv. Virus Res.* **2010**, *77*, 119–158, doi:10.1016/B978-0-12-385034-8.00005-3.
45. Dorokhov, Y.L.; Frolova, O.Y.; Skurat, E.V.; Ivanov, P.A.; Gasanova, T.V.; Sheveleva, A.A.; Ravin, N.V.; Mäkinen, K.M.; Klimyuk, V.I.; Skryabin, K.G.; et al. A Novel Function for a Ubiquitous Plant Enzyme Pectin Methylesterase: The Enhancer of RNA Silencing. *FEBS Lett.* **2006**, *580*, 3872–3878, doi:10.1016/j.febslet.2006.06.013.
46. Jarillo, J.A.; Piñeiro, M.; Cubas, P.; Martínez-Zapater, J.M.; Jarillo, J.A.; Piñeiro, M.; Cubas, P.; Martínez-Zapater, J.M. Chromatin Remodeling in Plant Development. *Int. J. Dev. Biol.* **2009**, *53*, 1581–1596, doi:10.1387/ijdb.072460jj.
47. Adams, D.J.; van der Weyden, L.; Mayeda, A.; Stamm, S.; Morris, B.J.; Rasko, J.E. ZNF265--a Novel Spliceosomal Protein Able to Induce Alternative Splicing. *J. Cell Biol.* **2001**, *154*, 25–32, doi:10.1083/jcb.200010059.

48. Ouyang, P. SRrp37, a Novel Splicing Regulator Located in the Nuclear Speckles and Nucleoli, Interacts with SC35 and Modulates Alternative Pre-mRNA Splicing in Vivo. *J. Cell. Biochem.* **2009**, *108*, 304–314, doi:10.1002/jcb.22255.
49. Hudson, W.H.; Ortlund, E.A. The Structure, Function and Evolution of Proteins That Bind DNA and RNA. *Nat. Rev. Mol. Cell Biol.* **2014**, *15*, 749–760, doi:10.1038/nrm3884.
50. Villao-Uzho, L.; Chávez-Navarrete, T.; Pacheco-Coello, R.; Sánchez-Timm, E.; Santos-Ordóñez, E. Plant Promoters: Their Identification, Characterization, and Role in Gene Regulation. *Genes* **2023**, *14*, 1226, doi:10.3390/genes14061226.
51. Hanford, H.E.; Von Dwingelo, J.; Abu Kwaik, Y. Bacterial Nucleomodulins: A Coevolutionary Adaptation to the Eukaryotic Command Center. *PLOS Pathog.* **2021**, *17*, e1009184, doi:10.1371/journal.ppat.1009184.
52. Schneider, C.A.; Rasband, W.S.; Eliceiri, K.W. NIH Image to ImageJ: 25 Years of Image Analysis. *Nat. Methods* **2012**, *9*, 671–675.
53. Pfaffl, M.W. A New Mathematical Model for Relative Quantification in Real-Time RT-PCR. *Nucleic Acids Res.* **2001**, *29*, e45, doi:10.1093/nar/29.9.e45.